Ceramics International 49 (2023) 14834–14843

Contents lists available at ScienceDirect

Ceramics International

journal homepage: www.elsevier.com/locate/ceramint

Influence of AC fields and electrical conduction mechanisms on the flash-onset temperature: Electronic ($BiFeO_3$) vs. ionic conductors (8YSZ)

Sandra Molina-Molina [a], Antonio Perejón [a,b,**], Luis A. Pérez-Maqueda [a,***], Pedro E. Sánchez-Jiménez [a,b,*]

[a] Instituto de Ciencia de Materiales de Sevilla, Consejo Superior de Investigaciones Científicas-Universidad de Sevilla, Calle Américo Vespucio 49, Sevilla, 41092, Spain
[b] Departamento de Química Inorgánica, Facultad de Química, Universidad de Sevilla, Sevilla, 41012, Spain

ARTICLE INFO

Keywords:
Flash sintering
Alternating current
$BiFeO_3$
YSZ

ABSTRACT

This work aims to clarify the influence of AC (up to 50 kHz) vs DC fields on the flash-onset temperature, emphasizing the role of the electrical conduction mechanism. $BiFeO_3$ (BFO) is used as an example of electronic conductor while 8-mol % Yttria-stabilized zirconia (8YSZ) is used as an example of ionic conductor. For 8YSZ, a frequency dependence of the flash-onset temperature and flash-induced heating is observed. This is consistent with the different contributions found in the total electrical response of 8YSZ as characterized by impedance spectroscopy measurements. Estimations based on the blackbody radiation model suggest that 8YSZ samples attain higher temperatures under AC fields due to a more efficient heating. Moreover, a noticeable decrease in the activation energy for the electrical conduction after the flash is triggered is attributed to electronic conduction. Meanwhile, the lack of frequency response and insensitiveness to the type of electrical field found in the case of BFO can be attributed to its mainly electronic bulk conduction.

1. Introduction

Flash Sintering (FS) is a recently proposed field assisted densification technique, first devised by Rishi Raj and coworkers in a seminal work in 2010 [1]. They observed that Yttria-stabilized zirconia (YSZ) could be sintered at greatly reduced temperatures in just a few seconds when heated under a moderate electric field. At a certain gate temperature, which depends on the applied electric field strength, a dramatic drop of the electrical resistance fosters a power surge as the electrical current passing through the specimen abruptly increases [1]. The flash event is accompanied by a dramatic densification of the ceramic specimen and intense optical emission [1–3]. Since its proposal, FS has aroused substantial interest due to its scientific and technological significance [4–6]. It shows promise as a novel energy-efficient method to consolidate ceramic powders but also as a tool to facilitate the preparation of hard-to-sinter ceramics. While initially demonstrated in YSZ, it has quickly extended to the preparation of a broad class of oxide ceramic materials, typically displaying a negative coefficient temperature of resistivity (NTCR). Thus, predominantly electronic semiconductors [7–10], ionic conductors [3,11], and even insulator dielectric oxides [12–15] have all been sintered by FS.

An important research effort is currently being devoted to comprehend the flash-related phenomena and identify the underlying mechanisms responsible for triggering the flash [16–20]. It is now widely accepted that Joule heating plays a major role; the abrupt power surge essentially occurs when the current traversing through the specimen generates more heat than it can be dissipated [18,19]. Nevertheless, it is also clear that the Joule heating alone does not suffice to explain all the other phenomena concurrent to the flash [21,22], such as enhanced mass transfer kinetics [3,23], luminescence [24], defect generation [12,15,25] and the formation of unusual phases [26–28].

The first studies in FS were carried out using DC power supplies. Diverse directional field effects were quickly observed, depending on the conduction mechanism of the material [5]. In ionic conductors such as

* Corresponding author. Instituto de Ciencia de Materiales de Sevilla, Consejo Superior de Investigaciones Científicas-Universidad de Sevilla, Calle Américo Vespucio 49, Sevilla, 41092, Spain.
** Corresponding author. Instituto de Ciencia de Materiales de Sevilla, Consejo Superior de Investigaciones Científicas-Universidad de Sevilla, Calle Américo Vespucio 49, Sevilla, 41092, Spain.
*** Corresponding author.
E-mail addresses: aperejon@us.es (A. Perejón), maqueda@cica.es (L.A. Pérez-Maqueda), pedro.enrique@icmse.csic.es (P.E. Sánchez-Jiménez).

https://doi.org/10.1016/j.ceramint.2022.06.242
Received 27 February 2022; Received in revised form 21 June 2022; Accepted 22 June 2022
Available online 1 July 2022

YSZ and semiconductors such as ZnO and TiO_2, flashed specimens tend to develop heterogeneous microstructures. Substantial temperature gradients along the sample and electrochemical reduction processes lead to abnormal grain growth in the cathode [29] and anode respectively [10,19]. Moreover, asymmetric electrical resistance and temperature distribution while applying DC fields in soda lime glass have been attributed to the formation of a depletion layer in the anode [30]. Polarity induced Peltier effect has also been reported in the case of TiO_2 [31]. It was only natural that FS under AC fields was readily explored as a way to avoid such problems, as the migration of ions in the field direction is prevented [32]. Commonly, intermediate values of frequency up to 1 kHz [33] are employed to carry out AC-FS. Frequencies as low as 0.1 Hz [34] as well as fields of several GHz [35] have been shown to trigger the flash-event.

Several works have suggested that the use of AC fields helps to reduce temperature gradients and avoid oxygen depletion at the cathode [26,36], allowing for finer grain sizes and microstructural homogeneity [36]. Other authors also claim that the flash-onset significantly changes under AC fields [37,38].

So far, the results published are inconclusive or even contradictory. A reason for these discrepancies might be the different specimen geometry, experimental set-ups, or even the electrode materials used [39,40]. Furthermore, the measurement of the temperature has aroused some debate in the FS literature. Frequently, the real temperature of the sample is not closely monitored, so that just the furnace temperature is provided. Both pyrometer and IR thermal cameras have been used to estimate the surface temperature of the specimen undergoing the flash. *In situ* measurements using energy dispersive X-ray diffraction with synchrotron radiation have been used to analyze temperature heterogeneities during the flash event [31]. To overcome the uncertainty in the measurements, several authors have proposed different models to determine the flash-onset by assuming that thermal runaway is the main driving force for the flash [18,19].

Here, we attempt to clarify the influence of AC fields at different frequencies on the flash-onset temperature of two different materials displaying distinct electrical conduction mechanisms: $BiFeO_3$ as an example of an essentially electronic conductor, and YSZ as a well-known model of ionic conductor. To minimize the effect of sample heterogeneities in terms of the grain boundary constriction resistance [41] and stress the influence of the type of electrical conduction mechanism, flash experiments were conducted using previously densified specimens. The flash phenomenon is not exclusive of green bodies and has been studied for dense ceramics in order to remove the densification contribution to the electrical conductivity [24,42,43]. The present work focusses on the triggering of the flash event itself, not on the associated densification.

Flash experiments were carried out using DC and AC electric fields. In the latter case, frequencies as high as 50 kHz were tested. A comprehensive study of the electrical conductivity evolution during the flash-induced heating and its relationship with the predominant conduction mechanism is also offered. The effect of temperature measurement was assessed comparing different methods to determine the temperature of the flashing sample.

2. Materials and methods

Commercially available oxides (Fe_2O_3 (Sigma–Aldrich 310050, ≥99% purity), Bi_2O_3 (Sigma–Aldrich 223,891, 99.9% purity)) and 8 mol % Yttria-stabilized zirconia (8YSZ) (Tosoh Corporation, TZ-8Y) were used to prepare the specimens. $BiFeO_3$ (BFO) samples were synthesized by mechanochemistry. Stoichiometric amounts of the starting Fe_2O_3 and Bi_2O_3 oxides were placed in 80 cm^3 stainless steel jars with nine stainless steel balls 15 mm in diameter and were milled in a high-energy planetary mill (Fritsch Pulverisette 7) under 7 bar of oxygen pressure. More experimental details can be found in Ref. [44]. The starting powders were uniaxially pressed at 600 MPa into 3 mm diameter and 4 mm height cylindrical green bodies. Then, they were presintered before the flash experiments according to the following conditions: BFO at 850 °C for 1 min and 8YSZ at 1400 °C for 1 h. Heating and cooling were carried out at 10 °C min^{-1}. Specimen densities were determined according to the Archimedes principle. Presintered BFO had densities of 90% whereas presintered 8YSZ had 95% density after the sintering.

For the experiments, the samples were placed between two NiCr wires and then into a tubular furnace. The surface areas of the pellets in contact with the wires were coated evenly with Pt paste to ensure contact homogeneity at the electrodes. Two different power supplies were used to connect the wires: AST501A1 AMETEK Asterion (USA) for DC and 50 Hz-AC and PBZ80-5 KIKUSUI (Japan) for the 10 Hz and 50 kHz experiments. The temperature of the furnace was increased by means of a Eurotherm 3216 PID controller at a constant heating rate of 5 °C min^{-1} from room temperature up to the onset temperature of the flash event. The power supply was switched on at 500 °C and constant-voltage control mode was maintained until a pre-set current density limit was attained. At this point, the power supply automatically switched from voltage to current-controlled mode. Then, the power supply was promptly switched off and the furnace was allowed to cool down to room temperature. The values of the applied fields and current density limits were optimized before starting a series of experiments for each material. All flash experiments were performed under flowing synthetic air delivered from a cylinder. Electrical parameters were recorded with a power analyzer (PPA1500 Newtons 4th Ltd, UK). An industrial CCD camera (DMK 23U445 The Imaging Source GmbH, Germany) was used for visually monitoring the flash experiments. Thermal pictures of the samples during the experiments were captured by an infrared camera (PI 1 M, Optris GmbH, Germany). Impedance measurements of the flashed samples were performed using an impedance analyzer (PSM1735 Newtons 4th Ltd, UK) with an AC measuring voltage of 0.1 V.

2.1. Temperature measurement

In order to ascertain the thermal behavior of the samples during the flash process, a differential measurement system was devised (Fig. 1a). The cylindrical specimen was placed in a custom-built sample holder with a S-type thermocouple at about 1 mm away from the sample. A second thermocouple provided the environment or furnace temperature, $T_{furnace}$. As a way of example, Fig. 1b includes the typical temperature-time profile recorded in these experiments while Fig. 1c shows the electrical power density evolution. $T_{furnace}$ faithfully followed the linear heating program imposed. Meanwhile, T_{sample}, measured with the thermocouple placed close to the sample, progressively deviated due to Joule heating. When the flash was triggered, the sudden increase in temperature of the sample could be clearly noticed, as well as the rapid drop once the power supply was switched off. The plot also includes the estimation of the sample temperature according to the blackbody radiation model (T_{BB}), as it will be discussed hereafter.

3. Results and discussion

First, the effect of the type of electric field on the flash-onset of previously sintered specimens was evaluated. In the case of AC fields, frequencies ranging from 50 Hz to 50 kHz were explored. As ionic conduction is responsive to low frequencies, an additional experiment at 10 Hz was performed in the case of 8YSZ. The samples were heated at 5 °C min^{-1} while the current was continuously monitored. Upon reaching a preset current density limit, the power supply was readily switched off. Thus, the holding time of the flash in the steady state (Stage III) was negligible.

Flash experiments of BFO specimens were carried out under electric fields of 50 V cm^{-1} and a preset current density limit of 20 mA mm^{-2}. Fig. 2a shows the power density as a function of the sample temperature recorded for BFO flashed under AC and DC fields. Similar flash-onset temperatures were observed for all the experiments. Moreover, increasing the frequency of the AC field up to 50 kHz appears to have no

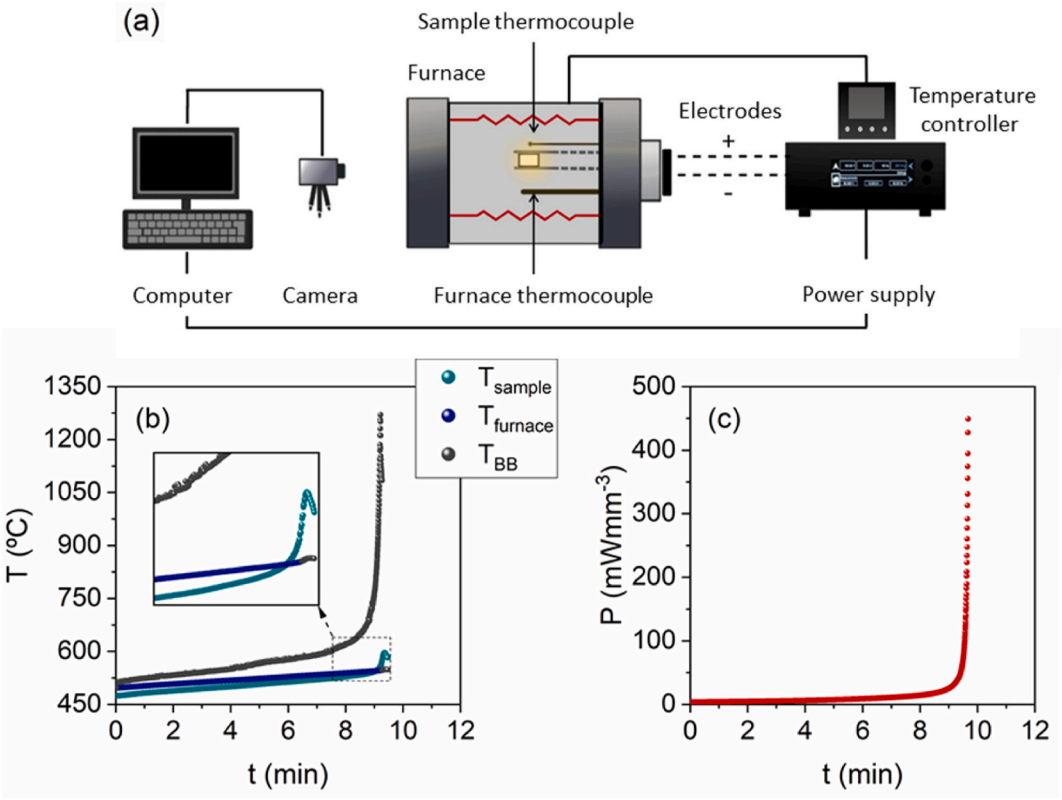

Fig. 1. (a) Scheme of the experimental device used to perform the flash experiments. (b) Temperature-time profiles and (c) corresponding power density profile recorded during an 8YSZ flash experiment carried out under a 50 kHz AC electric field of 70 V cm^{-1}, current density limit of 100 mA mm^{-2}.

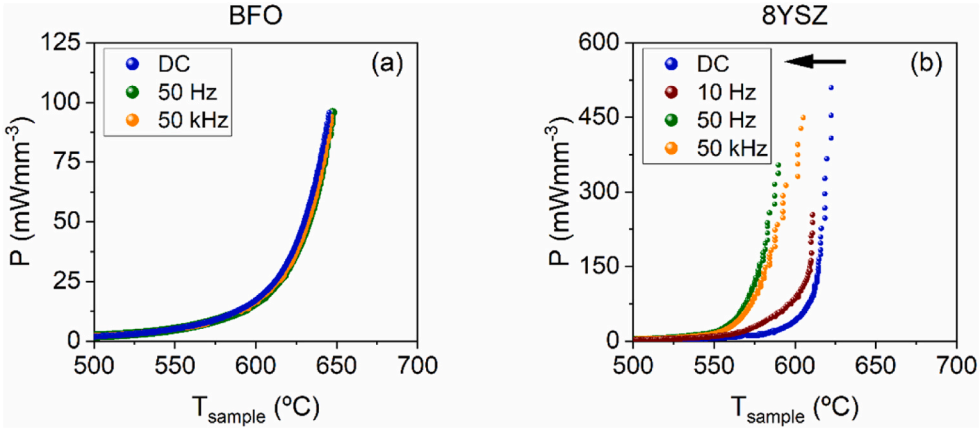

Fig. 2. Dissipated power density versus T_{sample} profiles recorded during flash experiments of predensified samples of (a) BFO under an electric field of 50 V cm^{-1}, current density limit of 20 mA mm^{-2} and (b) 8YSZ under an electric field of 70 V cm^{-1}, current density limit of 100 mA mm^{-2}. The arrow points the shift towards lower temperatures of the 8YSZ profiles as the frequency increases. All DC fields, 10Hz, 50 Hz and 50 kHz AC fields are compared.

noticeable influence. Arguably, the lack of influence of the frequency can be attributed to the mostly pure electronic conductivity of BFO [45]. In fact, impedance spectroscopy measurements (Fig. S1) revealed the electrical response of BFO as a single bulk contribution with associated capacitance values of 10^{-10}-10^{-9} F cm^{-1} [46] in the frequency range where the flash experiments were performed.

A completely different situation arises in the case of 8YSZ. The flash experiments were conducted under electric fields of 70 V cm^{-1} and a preset current density limit of 100 mA mm^{-2}. The dissipated power density versus sample temperature profiles, shown in Fig. 2b, evidence that the flash-onset temperature depends on the type of field employed.

According to the plots, while the flash triggers at a T_{sample} of about 610 °C under a DC field, the onset shifts down to about 560 °C under AC fields beyond 50 Hz. For the 10 Hz experiment, the flash-onset has an intermediate value of approximately 590 °C. The increase of the alternating field frequency lowers the flash-onset temperature from DC to 50 Hz. Above this value, the frequency seems to no longer have significant effect on the onset, which is observed at similar temperatures in the experiments carried out under 50 Hz and 50 kHz AC fields.

Fig. 3 includes the plot of the electrical resistivity versus T_{sample} measured during all flash experiments. In the case of BFO, the resistivity profiles are quite similar regardless of the type of field applied. For 8YSZ, resistivity under an AC field is substantially smaller, thus facilitating the flash-onset. The increased DC resistivity can be attributed to the

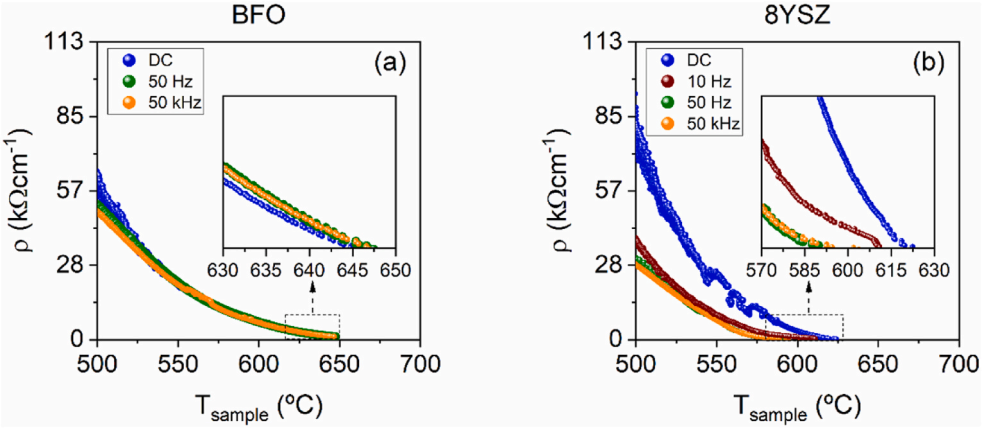

Fig. 3. Electrical resistivity as a function of T_{sample} measured during heating as the sample approaches the flash event for (a) BFO under an electric field of 50 V cm^{-1}, current density limit of 20 mA mm^{-2} and (b) 8YSZ under an electric field of 70 V cm^{-1}, current density limit of 100 mA mm^{-2}. The area close to the flash-onset is magnified in the inset plots.

electrode effects present in ionic conductors under an applied DC field. As amply reported, extensive contact driven reduction occurs at the positive electrode due to the migration of oxygen vacancies to the cathode and oxygen ions to the anode. Since the oxygen vacancies are removed by the electric field from the anode, a charge carrier depletion layer appears in this region. Consequently, the cathode acts as a partially blocking electrode [26,47,48] and the ionic charge transfer is restrained. The overall electrical resistivity of the sample increases thereby hindering the initiation of the flash as electrical conductivity gradients develop as well as temperature heterogeneity [49].

Three different contributions can be discerned in the electrical response of 8YSZ (Fig. S2) by impedance spectroscopy. At lower and intermediate frequencies, the conduction is dominated by the sample-electrode interface (capacitance values of 10^{-7}-10^{-5} F cm^{-1}) and by the grain boundary (capacitance values of 10^{-11}-10^{-8} F cm^{-1}). At higher frequencies, the conduction is associated to the bulk with capacitances in the order of 10^{-12} F cm^{-1} [46]. In other words, the blocking effect of the cathode is lost at higher frequencies, as well as the rest of electrode effects. Thus, the behavior of flash experiments in 8YSZ could be explained as the frequency-dependent effect of different contributions to the total electrical response.

Fig. 4 shows a sequence of IR pictures of the samples near the flash-onset. A homogeneous, field-independent superficial temperature distribution appears for BFO. In this case, the flash starts in the center of the sample and gradually extends to both electrodes. For 8YSZ, temperature gradients between anode and cathode are noticeable in the thermal

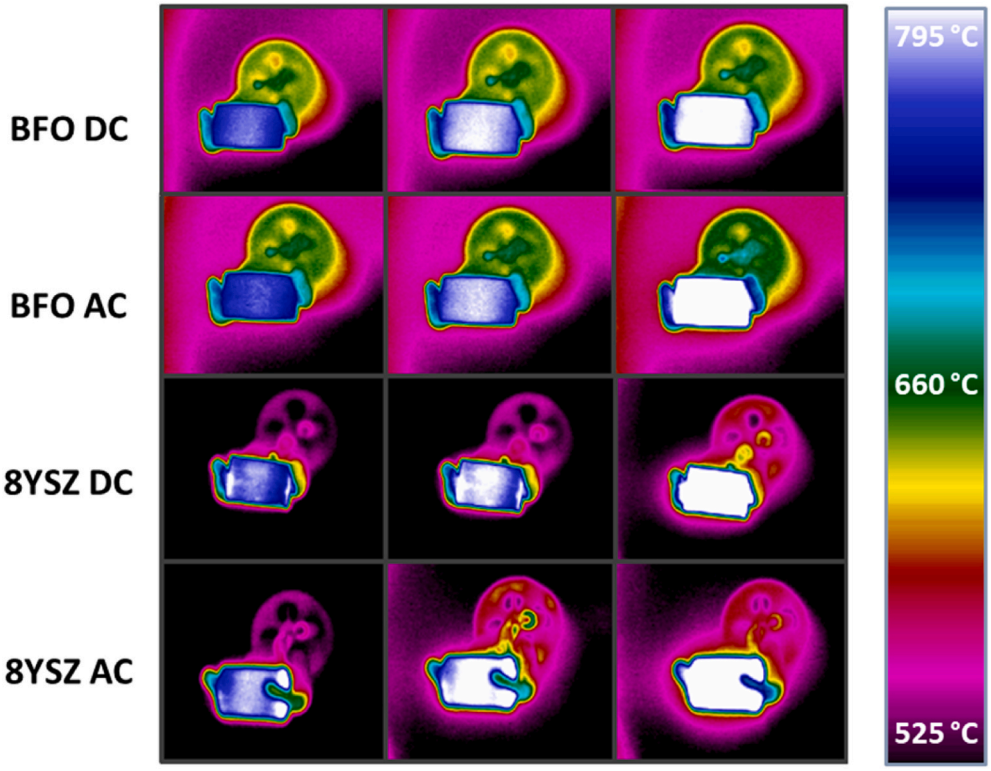

Fig. 4. IR images showing the temperature distribution across the surface of BFO and 8YSZ samples. The pictures were taken once the flash event was triggered, under both DC and AC-50 Hz fields. An electric field of 50 V cm^{-1}, current density limit of 20 mA mm^{-2} was applied for BFO; 8YSZ was flashed under an electric field of 70 V cm^{-1}, current density limit of 100 mA mm^{-2}.

images. While the DC-induced flash event in 8YSZ starts on the cathode and leads to asymmetrical heating throughout the specimen, a more homogeneous flash occurs under the application of an AC field.

Electro-coloration phenomena have been attributed to the activation of electronic conduction by the partial reduction induced in 8YSZ when applying DC and low frequency fields [34]. The presence of electronic conduction in typically ionic-conducting ceramics will be discussed in further detail below. Fig. 5 includes images of flashed 8YSZ samples. The evident blackening observed in the specimen flashed under a DC field is absent when an AC field is used instead. It is worth pointing out that the blackening mainly occurs before the thermal runaway rises uncontrolled, as it is noticeable even if the power supply is switched off before the transition to Stage III. This observation is in agreement with the results reported by Alvarez et al. on the DC electrical degradation of 8YSZ. They found that the blackened areas appeared prior to the drastic resistance drop associated with the flash event [50].

These electrochemical effects can be considerably minimized by using AC fields, due to the rapidly switching polarity of the electrodes which prevents the accumulation of oxygen vacancies. The fact that no effect of the frequency is observed over 50 Hz can be attributed to the ionic conductivity of 8YSZ. Even 50 Hz is probably too-high frequency to produce significant response.

To further study the effects of DC fields on the flash process depending on the type of electrical conduction mechanism, a series of flash experiments were consecutively conducted on the same specimen. Fig. 6 includes the power density profiles of all these experiments. After each flash, the sample was let to cool down to 500 °C before initiating a new flash experiment. The flash-onset remains invariant in BFO (Fig. 6a) but consistently shifts to lower temperatures for the 8YSZ sample (Fig. 6b).

Because of its essentially electronic conduction, no substantial changes in the electrical conductivity of the BFO specimen were induced by the flash event. For 8YSZ, it has been reported in previous studies that flashed specimens exhibit higher electrical conductivity when compared to the pre-flashed state and to conventionally sintered samples. This enhanced conductivity is not attributable to densification but to the creation of mobile vacancies [51]. Even for already densified samples, as the flash-onset temperature depends on sample conductivity, subsequent flashes conducted on the same sample initiated at progressively lower temperatures for 8YSZ as a consequence of the changes in the defect structure caused by DC flash. For other ionic conductors like gadolinium doped ceria, increased conductivity has been reported after repeating flash experiments on the same sample [52].

It is generally acknowledged that the flash is triggered by a thermal runaway produced by Joule heating: the rise in temperature due to the flow of current leads to an increase in conductivity that further increases the current density at a constant applied field [18,19]. Eventually, once a critical combination of electrical conductivity (σ) and its rate of change with temperature (dσ/dT) is attained, more heat is generated by Joule heating than it can be dissipated to the environment. In order to establish a consistent comparison of the flash-onset temperatures in the different experiments, the thermal-runaway model proposed by Luo et al. was employed [19]. Luo's model is based upon the temperature dependence of electrical conductivity. Thus, the thermal runaway condition is determined by the following expression [19]:

$$E^2 V_s \left.\frac{d\sigma}{dT}\right|_{T_s} > 4\sigma_{Stefan} T_s^3 A_s \quad (1)$$

Where V_s is the total volume of the specimen, E is the applied electric field, σ is the specimen electrical conductivity, T_S is the specimen temperature, A_S is the surface area of the specimen and σ_{Stefan} is the Stefan–Boltzmann constant ($\sigma_{Stefan} = 5.67 \times 10^{-8}$ W m^{-2} K^{-4}). The same heat exchange on the whole surface area of the cylindrical pellets was considered. Emissivity was considered to be equal to 1. The left-hand side of Eq. (1) accounts for the heat generation rate while the right-hand side represents the dissipation rate assuming blackbody radiative heat transfer. The temperature value T_S satisfying Eq. (1) is a reasonable estimation of the flash-onset temperature. Graphically, if both sides of Eq. (1) are plotted versus the specimen temperature, the cross between plots indicates the flash-onset temperature as shown in Fig. 7.

Difficult to quantify experimentally, the blackbody radiation model is normally used as an approximation to estimate T_s [19]:

$$T_s = \left(T_0^4 - \frac{W}{A_s \sigma_{Stefan}}\right)^{1/4} \quad (2)$$

Where T_0 is the furnace temperature and W is the electric power. The applicability of the blackbody radiation model to estimate sample temperature has aroused some debate, as it disregards heat convection and conduction and assumes a stable steady state, what certainly is not entirely valid in flash experiments, especially during Stage II when the flash-onset is reached. On one hand, assuming that all electrical power is converted to thermal radiation could lead to temperature overestimation. On the other hand, the assumption of the flashing sample as a perfect emitter and the derivation of T_s from Eq. (2) as the surface temperature of the sample might also affect the reliability of the temperature estimation. The possibility of temperature heterogeneity appearing across the specimen needs to be properly addressed when using the blackbody radiation model for materials like 8YSZ under the influence of a DC field. Moreover, thermal gradients are also usual in

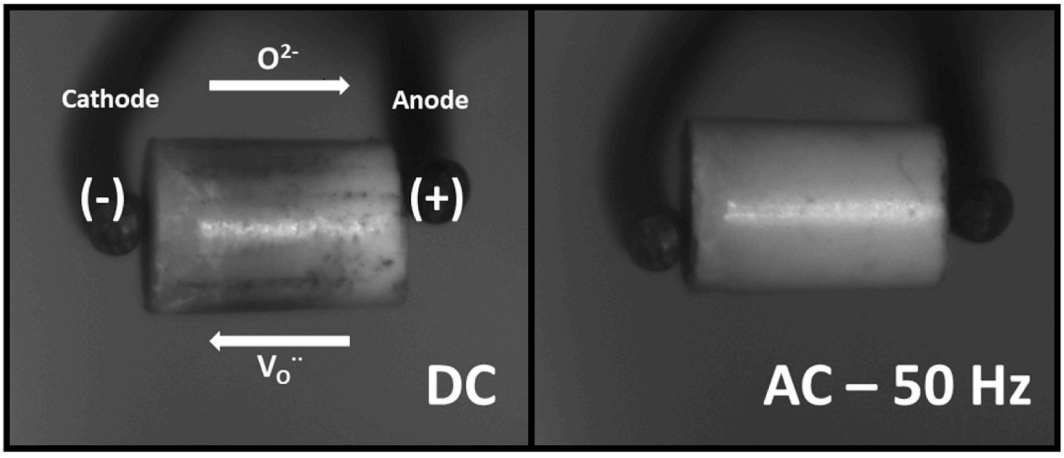

Fig. 5. Optical images of flashed 8YSZ samples using DC and 50 Hz-AC fields of 70 V cm^{-1}. Electrochemical blackening caused by DC is evident while the AC-flashed sample retains its original color. DC electrode polarity as well as cathodic/anodic areas of the sample are identified; charged species flow is also depicted.

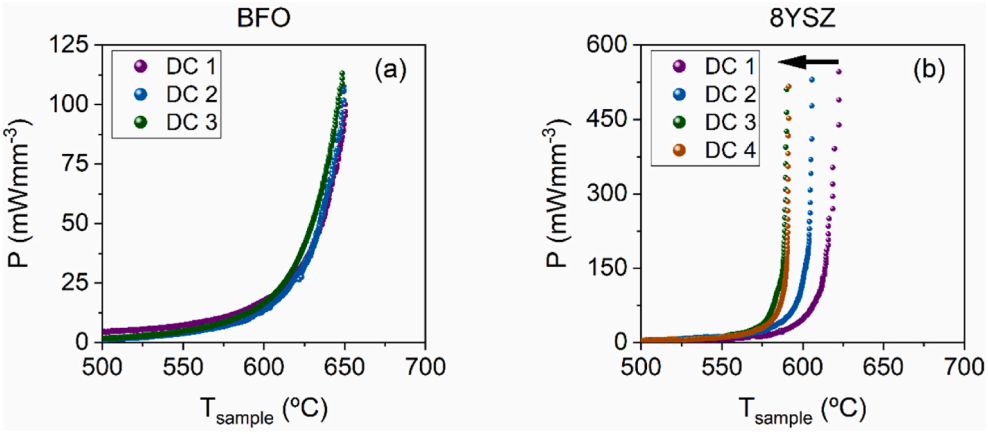

Fig. 6. Power density versus sample temperature plots recorded for consecutive flashes induced on the same specimens of (a) BFO under an electric DC field of 50 V cm^{-1}, current density limit of 20 mA mm^{-2} and (b) 8YSZ under an electric DC field of 70 V cm^{-1}, current density limit of 100 mA mm^{-2}. The number of each DC flash indicates the order in which the experiments were performed.

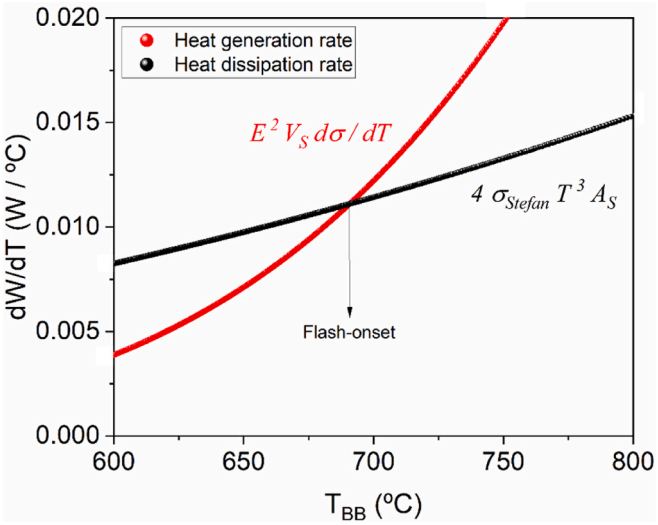

Fig. 7. Heat generation and dissipation rates plotted against blackbody temperature of the specimen. The curves have been computed using the experimental data from a BFO-DC experiment under an electric DC field of 50 V cm^{-1}, current density limit of 20 mA mm^{-2}. The flash-onset is the temperature which meets the thermal runaway condition as described by Eq. (1).

cylindrical pellets of reduced dimensions [39].

However, despite the doubts cast, the blackbody radiation model has been shown to provide reasonably accurate estimations [2]. Table 1 includes the flash-onset temperatures as calculated by Luo's method as well as the temperature measured at that very same time by the thermocouple next to the flashing specimen.

Table 1
Estimated blackbody flash-onset temperatures and corresponding temperatures measured at that same time by the thermocouple placed next to the flashing sample.

Material	f (Hz)	Estimated T_{Onset} (blackbody) (°C)	Estimated T_{Onset} (thermocouple) (°C)
BFO	0	695	618
	50	701	623
	$50{\cdot}10^3$	699	622
8YSZ	0	686	590
	10	703	572
	50	715	559
	$50{\cdot}10^3$	716	563

In the case of BFO, the flash-onset temperatures estimated by the model appear to be independent of the type of electric field, in agreement with the flash-onset observed in the power vs. sample temperature plots (Fig. 2a). Nevertheless, the temperature estimated by the model is about 80 °C higher. The difference is reasonable if we consider the limitations of the model as well as the rapid heating once the flash is triggered, which must produce considerable temperature gradients around the sample thus influencing the thermocouple measurement accuracy.

Contrarily, the 8YSZ specimen exhibits once again differences between AC and DC flash-onset temperature. The gap between measured and estimated temperature rises to about 100 °C for the DC experiment and even to 160 °C when the flash is induced by an AC field. The effect of frequency on the flash-onset is evidenced from DC to 50 Hz but disappears with higher frequency, as estimated flash-onset for both 50 Hz and 50 kHz experiments is basically the same.

Moreover, the predicted temperatures contradict the lower flash-onset values measured by the thermocouple, as evidenced in Fig. 2b. According to the model, higher flash-onset temperatures are attained under AC fields. This apparent discrepancy indicates a steeper increase in sample temperature due to Joule heating occurs in AC; consequently, the flash-onset is observed at a lower thermocouple temperature. Considering the previously described electrode effects and electrical conductivity gradients associated to DC flash in 8YSZ, the thermal runaway condition could be locally satisfied due to a heterogeneous flash starting in the cathode, thus explaining the lower predicted flash-onset when compared to AC. This suggests AC fields allow for a more efficient power-to-heat conversion in 8YSZ, since thermal runaway happens in a sample with homogeneous temperature distribution.

To further investigate the influence of frequency and the electrical conduction mechanism in the flash process, the evolution of the electrical conductivity was studied. In Fig. 8, the logarithm of the measured conductivity is plotted against the inverse of the blackbody sample temperature as determined by Eq. (2) for DC and AC-50 Hz experiments. Activation energies were obtained for all experiments (Figs. S3 and S4).

Assuming time-independent ohmic behavior and an Arrhenius dependence of the electrical conductivity with temperature, it follows that:

$$\sigma = \sigma_0 exp\left(-\frac{E_a}{k_B T}\right) \quad (3)$$

Where σ is the electrical conductivity, k_B the Boltzmann constant and E_a the activation energy for the electrical conduction.

This law is frequently used to fit conductivity data for both BFO and 8YSZ in the context of electrical properties and Flash Sintering [45,51].

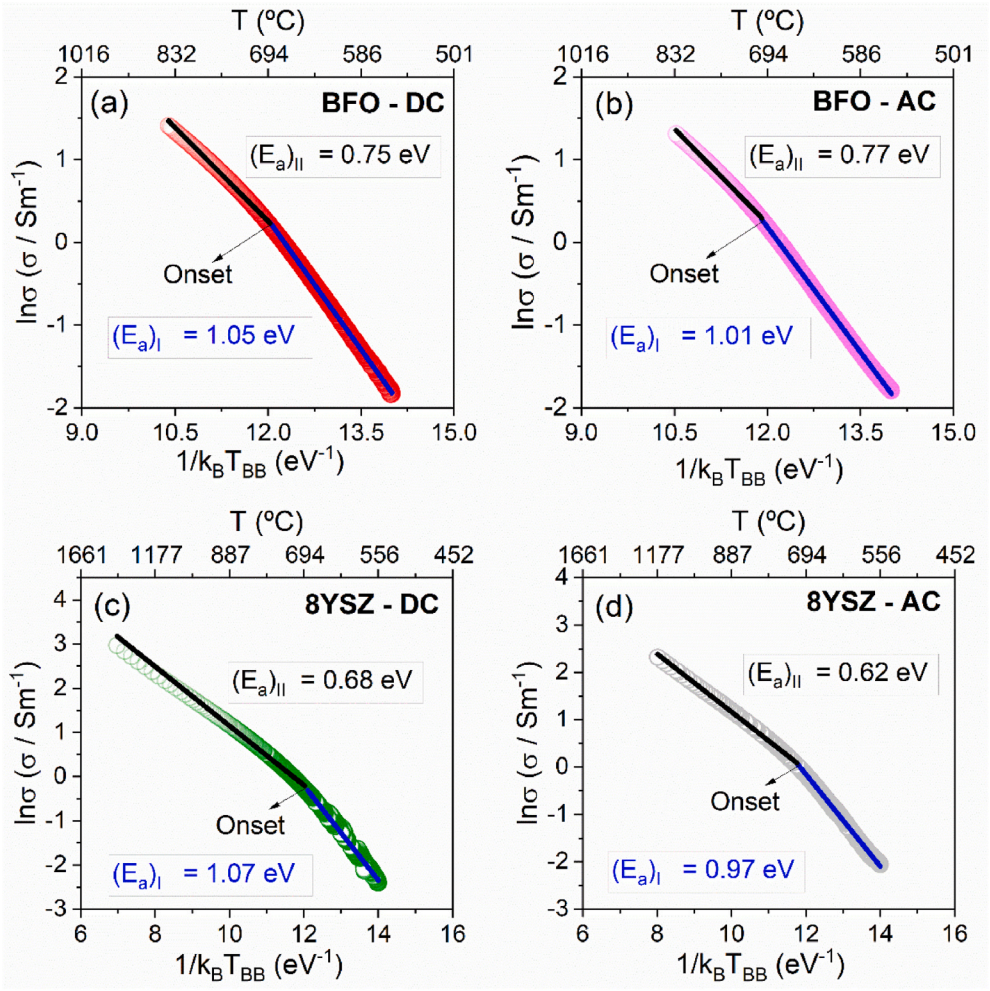

Fig. 8. Evolution of electrical conductivity as a function of the reverse of the blackbody temperature for (a) BFO-DC, (b) BFO-AC 50 Hz, (c) 8YSZ-DC and (d) 8YSZ-AC 50 Hz experiments, measured during heating as the sample approaches the flash event. An electric field of 50 V cm^{-1}, current density limit of 20 mA mm^{-2} was applied for BFO; 8YSZ was flashed under an electric field of 70 V cm^{-1}, current density limit of 100 mA mm^{-2}. The activation energies for Stage I and Stage II were derived for all experiments from the linear fittings before and after the flash-onset, respectively.

Below the flash-onset, all estimations show good agreement with the reported values for BFO [8] and 8YSZ [53]. However, a deviation from the linear trend appears during all our flash experiments as pictured in Fig. 8. Even so, two distinct linear regions with different slopes can be discerned within the conductivity profiles as the temperature increases. Once the estimated flash-onset temperature is reached, the transition between both regions becomes evident, so they can be associated to the well-known flash stages.

Firstly, Stage I (incubation period) as the steeper slope – higher activation energy regime and thereafter, Stage II (flash event) corresponding to a decreased slope and lower activation energy. The effect of densification as suggested by some authors [54] is dismissed in this discussion, since this apparent non-linearity is observed in already dense specimens.

After the onset, there is a significant change in the activation energy in the case of 8YSZ. Actually, this bending of the conductivity curve for YSZ has been previously investigated in several studies. Different explanations are proposed, all of them considering that a single activation energy is not enough to explain the temperature dependence of the electrical conductivity in YSZ. One approach describes the existence of two distinct temperature regimes for the activation energy, associated to temperature dependent interactions in the defect structure, whether in terms of trapped vacancies [55] or different height potential barriers [56]. Estimated activation energies are in the range of $E_a = 1.1$ eV for the low temperature region and $E_a = 0.6$ eV for the high temperature region, while the transition takes place over a wide temperature range between 650 °C and 1000 °C [56]. Our estimations are in excellent agreement with these values. In addition, the non-linear behavior of the conductivity in YSZ can also be explained as the combined contribution of intrinsic vacancies and field-generated vacancies [57]. In any case, oxygen transport is considered to be responsible for the electrical conduction despite the changes in the activation energy.

However, a decreased E_a could also be regarded not only as a result of a higher concentration and/or higher mobility of oxygen vacancies, but also as a change in the conduction mechanism. Understanding the activation energy as the minimum amount of energy required to *activate* the transport of the charge carriers, the diminished values of E_a once the flash is triggered could be a sign of electronic transport.

There is strong evidence of electronic conduction in 8YSZ. It has been proposed that electrochemical reduction does not generate enough vacancies to explain the decrease in the activation energy, but it can trigger the transition to electronic conduction [50]. The high mobility of electronic carriers has a great impact on the overall conductivity of the sample. Electronic conduction in 8YSZ has been reported when applying a small DC bias [58] and also while performing flash experiments [59]. Very recently, the decrease in the activation energy of 3YSZ during Flash Sintering was attributed to an important electronic contribution [60].

For our 8YSZ experiments, the activation energy was found to be higher for the lowest explored frequencies (DC and 10 Hz). This could be attributed to the ionic motion being restrained by the electrode effects previously discussed in this text, which become less and less significant as the frequency increases. After the flash-onset, the smaller variation of E_a with frequency as compared to the pre-onset values could indicate the presence of the aforementioned electronic contribution, less sensitive to frequency than ionic conduction.

The activation energy for electronic carriers in 8YSZ is notably

higher than the energy required for oxygen transport in the lower temperature range where the flash experiments were initiated [61]. While ionic conduction might be responsible of the progressive resistance lowering eventually leading to flash, electronic conduction plays a remarkable role in the latter stages of FS, as it is activated once the flash-onset is reached. Another evidence for electronic conduction could reside in the decreased phase-shift between voltage and current when the flash is triggered (Fig. S5).

In Fig. 2b, the power profiles show a smooth growth for 50 Hz and 50 kHz and an almost vertical rise in the case of DC and 10 Hz. This might be caused by the presence of electronic conductivity at lower frequencies, producing a more abrupt increase in conductivity not present in AC at high frequency. Another hint of a different conduction mechanism being activated at lower frequencies could reside in the differences between the power densities at the flash-onset temperature (Table S1). Flash is triggered within a narrow range of power density between 10 and 50 mW mm^{-3} [62]. In the case of 8YSZ, lower power densities were found for the onset of DC and 10 Hz experiments, which might be consistent with the activation of electronic conduction.

For BFO instead, the relationship between conductivity and the reverse of the temperature remains closer to linearity. Changes with frequency in the activation energy are not significant. Still, the bending of the conductivity profiles is noticeable. One explanation could be the hypothesized flash-induced avalanche of Frenkel defects which injects carriers in the form of electron-hole pairs and enhances conductivity [16]. To the best of our knowledge, there is no evidence of non-linear conductivity in BFO, which is an electronic conductor with an almost intrinsic behavior [45]. Assuming then that Eq. (3) remains true over the whole temperature range, it can be inferred that the blackbody sample temperature is an overestimation of the real temperature of the sample.

This statement is perfectly consistent with the blackbody model limitations. Fig. 9 shows an example of a conductivity profile plotted against all our available temperature data: blackbody estimations and both sample and furnace thermocouple measurements. The evolution of conductivity with increasing temperature as measured by the two thermocouples is completely different, showing the typical “non-linear” flash profile. As opposed to estimated blackbody temperature, this could derive from the underestimation of temperature when using instruments like thermocouples to measure the temperature.

Compared to the furnace thermocouple, the thermocouple placed next to the sample gives a more realistic temperature measurement, thus resulting in a conductivity profile closer to linearity. The impact of the accuracy of temperature measurements in the conductivity study of flash experiments has been already addressed. For example, conductivity profile bending and decrease in activation energy from Stage I to Stage II was also found during FS of 3YSZ using the Pt-standard method to estimate the sample temperature instead of the blackbody radiation model [60].

Whether estimated or directly measured, the chosen temperature values are critical for the proper interpretation of the electrical conductivity behavior. Of course, this issue is also present for all our 8YSZ experiments, but their inherent non-linearity affects more drastically the conductivity profiles, so the effect of temperature overestimation is not as prominent as in BFO.

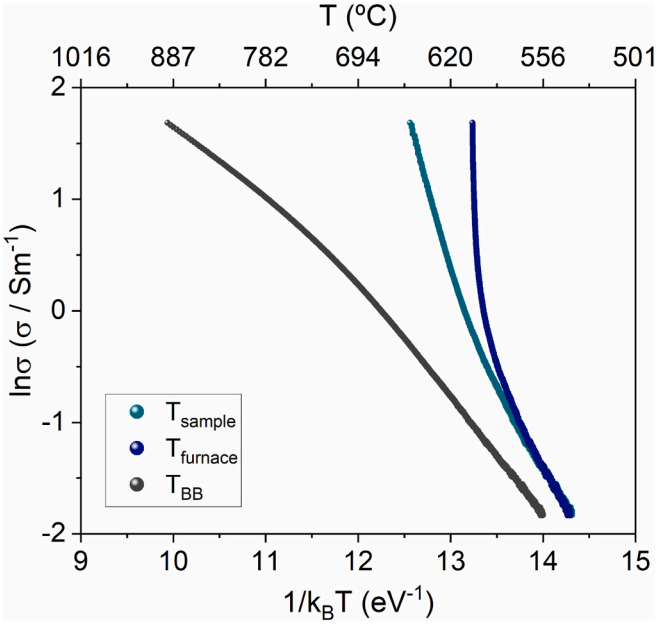

Fig. 9. Evolution of electrical conductivity as a function of the reverse of temperature for a BFO-DC flash experiment under an electric DC field of 50 V cm^{-1}, current density limit of 20 mA mm^{-2}, considering the values measured by the setup thermocouples and estimated using the blackbody radiation model.

4. Conclusions

This work presents a concise study on the influence of alternating fields and the electrical conduction mechanism on the flash-onset temperature and overall conductivity evolution during flash experiments. In a model ionic conductor, such as 8YSZ, the flash-onset depends on the frequency up to 50 Hz. Blackbody model estimations indicate that the 8YSZ samples attain higher temperatures with AC fields. This behavior could be attributed to a more homogeneous and efficient heating for ionic conductors flashed under AC fields. Above 50 Hz, no further effect of frequency is found on the flash-onset up to 50 kHz. In flash experiments performed under DC fields, electrode-related phenomena, such as electrochemical blackening and increased post-flash conductivity of the samples were observed due to redox reactions at the electrodes modifying the concentration of charge carriers and, therefore, the overall conductivity. Conversely, results for BFO show no significant differences between DC and AC fields because of its mainly electronic conduction.

The electrical conductivity of 8YSZ during the flash experiments follows a non-linear landscape, with two distinct regions, prior and after the flash. The noticeable decrease in the activation energy can be explained as an increase in the concentration and/or mobility of ionic carriers but also as a sign of electronic conduction. In addition, the frequency dependence of activation energy could indicate that frequency has an effect on balancing the ionic and electronic contributions in the likely scenario of mixed conduction in 8YSZ flash. Activation energy changes for BFO were not as significant, though a slight departure from linearity is observed. The apparent non-linearity is ascribed to a temperature overestimation by the blackbody radiation model.

All in all, the flash process in 8YSZ is dominated by field-induced electrode effects that progressively vanish with frequency while the electronic conduction of BFO remains basically insensitive to frequency. Although temperature measurement in FS is a challenging task and electrical transport in ceramics is a complex matter, precise temperature estimations as well as careful examination of electrical conduction seem to be crucial to better understand the ultimate mechanism driving Flash Sintering.

Declaration of competing interest

The authors declare that they have no known competing financial interests or personal relationships that could have appeared to influence the work reported in this paper.

Acknowledgements

This work has been funded by the grants CTQ2017-83602-C2-1-R (MCIN/AEI/10.13039/501100011033 and ERDF A way of making Europe by the European Union), projects P18-FR-1087 and US-1262507

(Junta de Andalucía-Consejería de Conocimiento, Investigación y Universidad – Fondo Europeo de Desarrollo Regional (FEDER) (Programa Operativo FEDER Andalucía 2014–2020) and INTRAMURAL-CSIC grant numbers 201960E092 and 202060I004.

Appendix A. Supplementary data

Supplementary data to this article can be found online at https://doi.org/10.1016/j.ceramint.2022.06.242.

References

[1] M. Cologna, B. Rashkova, R. Raj, Flash sintering of nanograin zirconia in <5 s at 850°C, J. Am. Ceram. Soc. 93 (2010) 3556–3559.
[2] K. Terauds, J.M. Lebrun, H.H. Lee, T.Y. Jeon, S.H. Lee, J.H. Je, R. Raj, Electroluminescence and the measurement of temperature during Stage III of flash sintering experiments, J. Eur. Ceram. Soc. 35 (2015) 3195–3199.
[3] H. Yoshida, Y. Sakka, T. Yamamoto, J.-M. Lebrun, R. Raj, Densification behaviour and microstructural development in undoped yttria prepared by flash-sintering, J. Eur. Ceram. Soc. 34 (2014) 991–1000.
[4] M. Biesuz, V.M. Sglavo, Flash sintering of ceramics, J. Eur. Ceram. Soc. 39 (2019) 115–143.
[5] M. Yu, S. Grasso, R. Mckinnon, T. Saunders, M.J. Reece, Review of flash sintering: materials, mechanisms and modelling, Adv. Appl. Ceram. 116 (2017) 24–60.
[6] E. Gil-González, L.A. Pérez-Maqueda, P.E. Sánchez-Jiménez, A. Perejón, Flash sintering research perspective: a bibliometric analysis, Materials 15 (2022) 416.
[7] A.L.G. Prette, M. Cologna, V. Sglavo, R. Raj, Flash-sintering of Co2MnO4 spinel for solid oxide fuel cell applications, J. Power Sources 196 (2011) 2061–2065.
[8] L.A. Pérez-Maqueda, E. Gil-Gonzalez, A. Perejon, J.-M. Lebrun, P.E. Sanchez-Jimenez, R. Raj, Flash sintering of highly insulating nanostructured phase-pure BiFeO3, J. Am. Ceram. Soc. 100 (2017) 3365–3369.
[9] Y. Zhang, J. Nie, J.M. Chan, J. Luo, Probing the densification mechanisms during flash sintering of ZnO, Acta Mater. 125 (2017) 465–475.
[10] Q. Wang, C.S. Watts, C.E. Athanasiou, Z. Dai, M. Hu, B.W. Sheldon, N.P. Padture, The effect of atmosphere on the flash-sintering of nanoscale titania ceramics, Scripta Mater. 199 (2021), 113894.
[11] M. Cologna, A.L.G. Prette, R. Raj, Flash-sintering of cubic yttria-stabilized zirconia at 750°C for possible use in SOFC manufacturing, J. Am. Ceram. Soc. 94 (2011) 316–319.
[12] A. Karakuscu, M. Cologna, D. Yarotski, J. Won, J.S.C. Francis, R. Raj, B. P. Uberuaga, Defect structure of flash-sintered strontium titanate, J. Am. Ceram. Soc. 95 (2012) 2531–2536.
[13] H. Yoshida, P. Biswas, R. Johnson, M.K. Mohan, Flash-sintering of magnesium aluminate spinel (MgAl2O4) ceramics, J. Am. Ceram. Soc. 100 (2017) 554–562.
[14] M. Biesuz, V.M. Sglavo, Flash sintering of alumina: effect of different operating conditions on densification, J. Eur. Ceram. Soc. 36 (2016) 2535–2542.
[15] M. Cologna, J.S.C. Francis, R. Raj, Field assisted and flash sintering of alumina and its relationship to conductivity and MgO-doping, J. Eur. Ceram. Soc. 31 (2011) 2827–2837.
[16] K.S. Naik, V.M. Sglavo, R. Raj, Flash sintering as a nucleation phenomenon and a model thereof, J. Eur. Ceram. Soc. 34 (2014) 4063–4067.
[17] R. Chaim, Particle surface softening as universal behaviour during flash sintering of oxide nano-powders, Materials 10 (2017) 179.
[18] R.I. Todd, E. Zapata-Solvas, R.S. Bonilla, T. Sneddon, P.R. Wilshaw, Electrical characteristics of flash sintering: thermal runaway of Joule heating, J. Eur. Ceram. Soc. 35 (2015) 1865–1877.
[19] Y. Zhang, J. Il Jung, J. Luo, Thermal runaway, flash sintering and asymmetrical microstructural development of ZnO and ZnO-Bi2O3 under direct currents, Acta Mater. 94 (2015) 87–100.
[20] W. Ji, B. Parker, S. Falco, J.Y. Zhang, Z.Y. Fu, R.I. Todd, Ultra-fast firing: effect of heating rate on sintering of 3YSZ, with and without an electric field, J. Eur. Ceram. Soc. 37 (2017) 2547–2551.
[21] R. Raj, Joule heating during flash-sintering, J. Eur. Ceram. Soc. 32 (2012) 2293–2301.
[22] O. Guillon, R.A. De Souza, T.P. Mishra, W. Rheinheimer, Electric-field-assisted processing of ceramics: nonthermal effects and related mechanisms, MRS Bull. 46 (2021) 52–58.
[23] J. Narayan, A new mechanism for field-assisted processing and flash sintering of materials, Scripta Mater. 69 (2013) 107–111.
[24] D. Yadav, R. Raj, Two unique measurements related to flash experiments with yttria-stabilized zirconia, J. Am. Ceram. Soc. 100 (2017) 5374–5378.
[25] T.P. Mishra, R.R.I. Neto, R. Raj, O. Guillon, M. Bram, Current-rate flash sintering of gadolinium doped ceria: microstructure and Defect generation, Acta Mater. 189 (2020) 145–153.
[26] S.K. Jha, H. Charalambous, H. Wang, X.L. Phuah, C. Mead, J. Okasinski, H. Wang, T. Tsakalakos, In-situ observation of oxygen mobility and abnormal lattice expansion in ceria during flash sintering, Ceram. Int. 44 (2018) 15362–15369.
[27] Y. Zhu, B. Ma, K. Wang, Z. Sun, K. Ren, Y. Wang, Electric field-assisted solid-state reaction of $BaCO_3$-TiO_2 system, J. Am. Ceram. Soc. 104 (2021) 6572–6578.
[28] J.M. Lebrun, T.G. Morrissey, J.S.C. Francis, K.C. Seymour, W.M. Kriven, R. Raj, Emergence and extinction of a new phase during on-off experiments related to flash sintering of 3YSZ, J. Am. Ceram. Soc. 98 (2015) 1493–1497.
[29] S.-W. Kim, S.G. Kim, J.-I. Jung, S.-J.L. Kang, I.-W. Chen, Enhanced grain boundary mobility in yttria-stabilized cubic zirconia under an electric current, J. Am. Ceram. Soc. 94 (2011) 4231–4238.
[30] L. Pinter, M. Biesuz, V.M. Sglavo, T. Saunders, J. Binner, M. Reece, S. Grasso, DC-electro softening in soda lime silicate glass: an electro-thermal analysis, Scripta Mater. 151 (2018) 14–18.
[31] H. Charalambous, S.K. Jha, X.L. Phuah, H. Wang, H. Wang, J.S. Okasinski, T. Tsakalakos, In situ measurement of temperature and reduction of rutile titania using energy dispersive x-ray diffraction, J. Eur. Ceram. Soc. 38 (2018) 5503–5511.
[32] C. Schmerbauch, J. Gonzalez-Julian, R. Röder, C. Ronning, O. Guillon, Flash sintering of nanocrystalline zinc oxide and its influence on microstructure and defect formation, J. Am. Ceram. Soc. 97 (2014) 1728–1735.
[33] H. Charalambous, S.K. Jha, J. Okasinski, T. Tsakalakos, Spectral analysis and temperature measurement during flash sintering under AC electric field, Materialia 6 (2019), 100273.
[34] M. Biesuz, L. Pinter, T. Saunders, M. Reece, J. Binner, V.M. Sglavo, S. Grasso, Investigation of electrochemical, optical and thermal effects during flash sintering of 8YSZ, Materials 11 (2018) 1214.
[35] Y.V. Bykov, S.V. Egorov, A.G. Eremeev, V.V. Kholoptsev, I.V. Plotnikov, K. I. Rybakov, A.A. Sorokin, On the mechanism of microwave flash sintering of ceramics, Materials 9 (2016) 684.
[36] X.L. Phuah, B. Yang, H. Charalambous, T. Tsakalakos, X. Zhang, H. Wang, Microstructure and defect gradients in DC and AC flash sintered ZnO, Ceram. Int. 47 (2021) 28596–28602.
[37] R. Umemura, T. Tokunaga, T. Yamamoto, Flash sintering for $BaTiO_3$ with square alternating current field including zero-field duration, J. Ceram. Soc. Japan. 128 (2020) 1018–1023.
[38] X. Su, Y. Jia, C. Han, Y. Hu, Z. Fu, K. Liu, Y. Yu, X. Yan, Y. Wang, Flash sintering of lead zirconate titanate ceramics under an alternating current electrical field, Ceram. Int. 45 (2019) 5168–5173.
[39] J.V. Campos, I.R. Lavagnini, J.G. Pereira da Silva, J.A. Ferreira, R.V. Sousa, R. Mücke, O. Guillon, E.M.J.A. Pallone, Flash sintering scaling-up challenges: influence of the sample size on the microstructure and onset temperature of the flash event, Scripta Mater. 186 (2020) 1–5.
[40] C. Hwang, J. Yun, Effect of processing conditions on the flash onset temperature in hydroxyapatite, Materials 14 (2021) 5229.
[41] A. Mikrajuddin, F.G. Shi, H.K. Kim, K. Okuyama, Size-dependent electrical constriction resistance for contacts of arbitrary size: from Sharvin to Holm limits, Mater. Sci. Semicond. Process. 2 (1999) 321–327.
[42] F. Zhu, X. Peng, J. Liu, D. Liu, K. Ren, Y. Wang, Surface temperature distribution on dense 8YSZ ceramics during the steady stage in AC flash sintering, Ceram. Int. 47 (2021) 2884–2887.
[43] J.A. Downs, Mechanisms of Flash Sintering in Cubic Zirconia, University of Trento, 2013.
[44] A. Perejón, N. Murafa, P.E. Sánchez-Jiménez, J.M. Criado, J. Subrt, M.J. Diánez, L. A. Pérez-Maqueda, Direct mechanosynthesis of pure $BiFeO_3$ perovskite nanoparticles: reaction mechanism, J. Mater. Chem. C 1 (2013) 3551–3562.
[45] M. Schrade, N. Masó, A. Perejón, L.A. Pérez-Maqueda, A.R. West, Defect chemistry and electrical properties of $BiFeO_3$, J. Mater. Chem. C 5 (2017) 10077–10086.
[46] D.C. Sinclair, Characterization of electro-materials using AC impedance spectroscopy, Bol. Soc. Esp. Cerám. Vidrio 34 (1995) 55–65.
[47] W. Qin, H. Majidi, J. Yun, K. van Benthem, Electrode effects on microstructure formation during FLASH sintering of yttrium-stabilized zirconia, J. Am. Ceram. Soc. 99 (2016) 2253–2259.
[48] S.E. Murray, T.J. Jensen, S.S. Sulekar, Y.-Y. Lin, N.H. Perry, D.P. Shoemaker, Propagation of the contact-driven reduction of Mn_2O_3 during reactive flash sintering, J. Am. Ceram. Soc. 102 (2019) 7210–7216.
[49] G.M. Jones, M. Biesuz, W. Ji, S.F. John, C. Grimley, C. Manière, C.E.J. Dancer, Promoting microstructural homogeneity during flash sintering of ceramics through thermal management, MRS Bull. 46 (2021) 59–66.
[50] A. Alvarez, Y. Dong, I.W. Chen, DC electrical degradation of YSZ: voltage-controlled electrical metallization of a fast ion conducting insulator, J. Am. Ceram. Soc. 103 (2020) 3178–3193.
[51] X. Vendrell, D. Yadav, R. Raj, A.R. West, Influence of flash sintering on the ionic conductivity of 8 mol% yttria stabilized zirconia, J. Eur. Ceram. Soc. 39 (2019) 1352–1358.
[52] T.P. Mishra, R.R.I. Neto, G. Speranza, A. Quaranta, V.M. Sglavo, R. Raj, O. Guillon, M. Bram, M. Biesuz, Electronic conductivity in gadolinium doped ceria under direct current as a trigger for flash sintering, Scripta Mater. 179 (2020) 55–60.
[53] M. Kilo, C. Argirusis, G. Borchardt, R.A. Jackson, Oxygen diffusion in yttria-stabilised zirconia - experimental results and molecular dynamics calculations, Phys. Chem. Chem. Phys. 5 (2003) 2219–2224.
[54] K.S. Naik, V.M. Sglavo, R. Raj, Field assisted sintering of ceramic constituted by alumina and yttria stabilized zirconia, J. Eur. Ceram. Soc. 34 (2014) 2435–2442.
[55] P.S. Manning, J.D. Sirman, R.A. De Souza, J.A. Kilner, The kinetics of oxygen transport in 9.5 mol % single crystal yttria stabilised zirconia, Solid State Ionics 100 (1997) 1–10.
[56] C. Ahamer, A.K. Opitz, G.M. Rupp, J. Fleig, Revisiting the temperature dependent ionic conductivity of yttria stabilized zirconia (YSZ), J. Electrochem. Soc. 164 (2017) 790–803.
[57] Y. Gao, F. Liu, D. Liu, J. Liu, Y. Wang, L. An, Electrical-field induced nonlinear conductive behavior in dense zirconia ceramic, J. Mater. Sci. Technol. 33 (2017) 897–900.
[58] N. Masó, A.R. West, Electronic conductivity in yttria-stabilized zirconia under a small dc bias, Chem. Mater. 27 (2015) 1552–1558.

[59] S. Jo, R. Raj, Transition to electronic conduction at the onset of flash in cubic zirconia, Scripta Mater. 174 (2020) 29–32.
[60] J.V. Campos, I.R. Lavagnini, V. Avila, B. Yoon, S. Ghose, R. Raj, E.M.J.A. Pallone, L. M. Jesus, On the Arrhenius-like behavior of conductivity during flash sintering of 3 mol% yttria stabilized zirconia ceramics, Scripta Mater. 203 (2021), 114093.
[61] L. Zhu, L. Zhang, A.V. Virkar, Measurement of ionic and electronic conductivities of yttria-stabilized zirconia by an embedded electrode method, J. Electrochem. Soc. 162 (2015) 298–309.
[62] R. Raj, Analysis of the power density at the onset of flash sintering, J. Am. Ceram. Soc. 99 (2016) 3226–3232.